

## Segregation-controlled nanocrystallization in an Al–Ni–La metallic glass

B. Radigue<sup>1</sup>, D. Blavette<sup>1</sup>, N. Wanderka<sup>2,a)</sup>, J. Banhart<sup>2</sup> and K. L. Sahoo<sup>3</sup>

<sup>1</sup>Université de Rouen-Groupe de Physique des Matériaux-UMR CNRS 6634, Avenue de l'Université BP 12, 76801 Saint Etienne du Rouvray, France

<sup>2</sup>Hahn-Meimer-Institut Berlin, Glienicker Str. 100, 14109 Berlin, Germany

<sup>3</sup>National Metallurgical Laboratory, Jamshedpur, India

(Received 9 January 2008; accepted 18 February 2008; published online 14 March 2008)

The early stages of devitrification of Al<sub>89</sub>Ni<sub>6</sub>La<sub>5</sub> metallic glass were investigated using three-dimensional atom probe. Even in the as-quenched amorphous state, nanometer-sized fluctuations of Ni and Al were observed. The Al-rich fluctuations act as nucleation sites for the crystallization at 443 K in which  $\alpha$ -Al clusters with a number density up to  $5 \times 10^{23} \text{ m}^{-3}$  nucleate and grow to nonspherical, 12 nm large crystals.  $\alpha$ -Al particles are almost pure in Al and are surrounded by a La-rich shell. It is concluded that La segregation controls the growth and limits the size of the  $\alpha$ -Al nanocrystals. © 2008 American Institute of Physics. [DOI: 10.1063/1.2897303]

Aluminum-based glasses containing transition metals and rare-earth elements such as nickel or lanthanum promise excellent mechanical properties such as outstanding strengths and corrosion resistance and are therefore of practical interest.<sup>1,2</sup> The yield strength is significantly increased by partial crystallization of fcc Al nanocrystals embedded in the amorphous matrix.<sup>3</sup> The high number density ( $>10^{21} \text{ m}^{-3}$ ) of nanocrystals originates from nuclei present in the as-quenched glass.<sup>4</sup> The stability of the Al-based amorphous phase as well as the pathway of crystallization are sensitive to the composition of these alloys.<sup>4–7</sup> Although nucleation and growth processes of Al nanocrystals have been investigated in several previous studies,<sup>8–12</sup> there is still a lack of understanding of the underlying processes. Both structure and local composition of amorphous and partially crystallized alloys have been analyzed by various scattering methods<sup>7,13</sup> and atom probe (AP) tomography,<sup>10,11</sup> where the latter technique is particularly suitable to study and analyze features on the nanometer scale.

We report on AP tomography measurements of the element distribution in amorphous Al<sub>89</sub>Ni<sub>6</sub>La<sub>5</sub>, both in the melt-spun (quenched) state and during primary crystallization in order to elucidate the early stages of crystallization and the role of the solute elements for nanocrystallization. Amorphous Al<sub>89</sub>Ni<sub>6</sub>La<sub>5</sub> ribbons of about 2 mm width and 30  $\mu\text{m}$  thickness were produced by single-roller melt spinning with a peripheral wheel velocity of 40 m/s. Differential scanning calorimetry of this material with a heating rate of 20 K/min indicated first crystallization at 458 K.<sup>7</sup> In order to observe the early stages of crystallization, the amorphous specimens were annealed at 443 K for 20 min and for 2 h. Details of specimen preparation will be described in Ref. 14. AP analyses were performed with a CAMECA three-dimensional (3D)-AP.<sup>15</sup> Additional information about the microstructure of the as-cast and the annealed material was obtained by transmission electron microscopy (TEM) and x-ray diffraction (XRD).

The amount of nickel in the as-quenched state as well as after heat treatment was found to be higher ( $\sim 8.3 \text{ at. } \%$ ) than the nominal composition, whereas the measured concentration of La ( $\sim 3.5 \text{ at. } \%$ ) was lower as evaluated by 3D-AP. These differences most likely arise from macroscopic fluctuations of concentration within the ribbons, e.g., between wheel and air side.

XRD analysis of the as-melt spun Al<sub>89</sub>Ni<sub>6</sub>La<sub>5</sub> ribbon reveals the featureless broad diffraction curve typical for amorphous solids (not shown). To further exclude the presence of small volume fractions of localized crystallites, TEM analysis at various locations of the ribbon was carried out. None of the diffraction patterns, one given in Fig. 1(a), indicated the presence of a crystalline phase. In contrast to diffraction, 3D-AP revealed many small compositional heterogeneities. Applying a cluster identification module<sup>16</sup> to reconstructed volumes shows small Ni-rich areas [Ni atoms marked as bold points in Fig. 1(b)]. Al-rich areas are also present but not as clearly visible as the Ni-rich areas since the concentration changes are smaller. Figure 1(c) shows the concentration depth profiles of Al, Ni, and La along the axis of the cylinder with 1.5 nm diameter marked in Fig. 1(a). La is randomly distributed. The mean chemical composition of the Ni-enriched areas (in at. %) is 85.7Al–11.5Ni–2.8La, with a maximum concentration of Ni up to  $\sim 25 \text{ at. } \%$ . The Al level varies from 70 to  $\sim 95 \text{ at. } \%$ . This shows that compositional fluctuations of two elements already exist in the as-cast material. The mobilities of both Al and Ni in the solidifying melt are obviously high enough to allow for such fluctuations, whereas the La atoms are quenched in on random positions. Similar compositional fluctuations were recently observed by AP analysis in several other as-quenched glasses including Al<sub>87</sub>–Ni<sub>5</sub>–La<sub>7</sub>–Zr<sub>1</sub> (Ref. 17) and Al–Ni–Yb.<sup>10</sup> Quenched-in Al nuclei were reported in Al–Ni–Y–Co glass.<sup>4</sup> It was proposed that such fluctuations could act as nuclei for primary crystallization during annealing.<sup>9</sup> Hence, a large number density of heterogeneities, in particular Ni-poor and Al-rich regions, is expected to give rise to a high number of  $\alpha$ -Al nanocrystals. This means that slight decomposition with respect to Ni and Al during solidification is crucial for  $\alpha$ -Al nucleation and not a deficiency of the quenching procedure.

<sup>a)</sup>Author to whom correspondence should be addressed. Tel.: +493080622079. FAX: +493080623059. Electronic mail: wanderka@hmi.de.

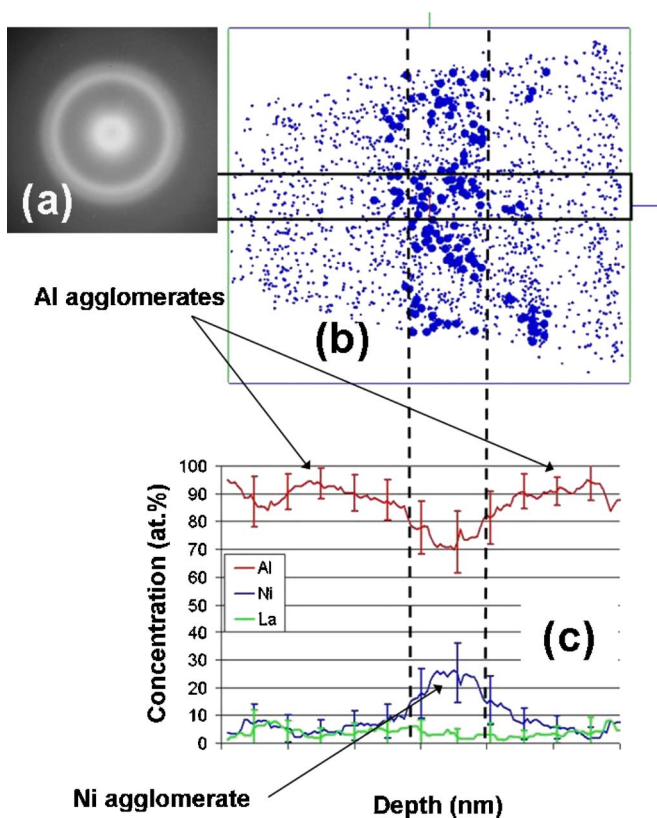


FIG. 1. (Color online) As-quenched  $\text{Al}_{89}\text{Ni}_6\text{La}_5$  metallic glass: TEM selected area diffraction pattern (a), elemental 3D-AP mapping of Ni atoms in a  $11 \times 11 \times 12 \text{ nm}^3$  volume (b). The bold dots in (b) represent Ni atoms in Ni-enriched regions defined by the criterion  $x_{\text{Ni}} > 10 \text{ at. \%}$ . Concentration depth profiles of all alloy constituents (c) along the axis of the marked cylinder in b. Arrows show where the Al concentration is above the average of 89 at. %.

Figure 2 shows 3D reconstructions of the atom positions in a volume of the alloy annealed at 443 K for 2 h. For the sake of clarity, only regions with more than 95 at. % Al and with more than 10 at. % La are represented in Figs. 2(b) and 2(c), respectively. The white space then corresponds to the part of the amorphous matrix containing less than these limits of Al or La. Irregularly shaped nonuniformities of the atom distributions are visible. La and Al agglomerates are correlated with each other, whereas Ni agglomerates are anticorrelated to Al. Specimens aged at the same temperature for just 20 min show a slightly less pronounced agglomeration.

TEM and XRD analyses of samples annealed for 20 min or 2 h revealed that the Al-rich agglomerates observed by

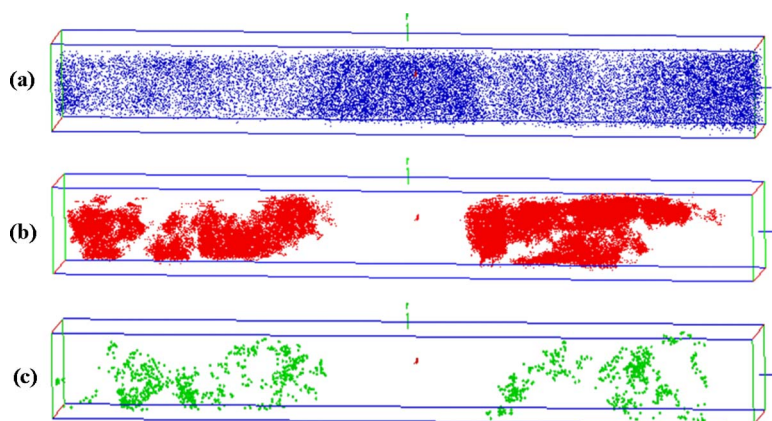


FIG. 2. (Color online) Perspective representation of the 3D-AP reconstruction of atoms in  $\text{Al}_{89}\text{Ni}_6\text{La}_5$  metallic glass annealed at 443 K for 2 h. (a) Ni, (b) Al, and (c) La. Analyzed volume is  $12 \times 12 \times 110 \text{ nm}^3$  large. A cluster-search module (Ref. 16) was used to show only Al atoms in regions with more than 95 at. % Al (b) and La atoms in regions containing more than 8 at. % La (c). Ni is shown without cluster selection since segregation is clearly visible in the full data set.

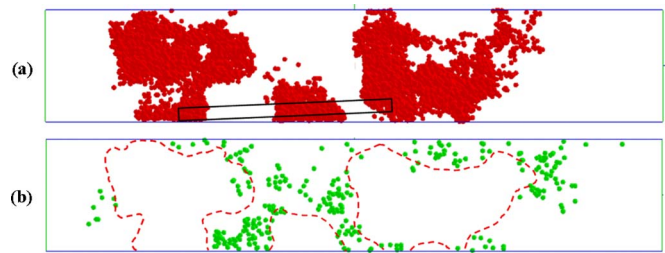


FIG. 3. (Color online) Atom map ( $9 \times 50 \text{ nm}^2$ ) in a specimen aged at 443 K for 2 h. Al atom positions in  $\alpha$ -Al crystal (Al concentration > 95 at. %) (a). La atom positions in the La-rich regions (La concentration > 10 at. %) (b).

3D-AP in Fig. 2(b) are clustered fcc  $\alpha$ -Al nanocrystals of nonspherical morphology.<sup>14</sup> Even after 2 h of annealing at 443 K, no evidence for the presence of crystalline phases other than  $\alpha$ -Al was found by TEM and by XRD. This is in accordance with the literature since  $\text{Al}_3\text{Ni}$  and  $\text{Al}_{11}\text{La}_3$  develop in the second crystallization stage at higher temperatures only.<sup>9</sup>

Composition, size, and number density of  $\alpha$ -Al clusters are derived from 3D-AP experiments. Again,  $\alpha$ -Al clusters are defined as regions where the concentration of Al exceeds the given limit of 95 at. %. The composition as well as the number density ( $\sim 5 \times 10^{23} \text{ m}^{-3}$ ) of  $\alpha$ -Al nanocrystals is independent of annealing time, whereas the mean size of  $\alpha$ -Al nanocrystals increases from about 6.4 nm after 20 min to about 12 nm after 2 h of aging. These values are averages over a rather wide size distribution of the irregularly shaped particles. This indicates that nucleation of the  $\alpha$ -Al particles occurs quickly, i.e., in less than 20 min. Since Ni-enriched areas and  $\alpha$ -Al clusters are anticorrelated, nucleation of  $\alpha$ -Al takes place in the Ni-depleted regions, after which  $\alpha$ -Al nanocrystals grow upon annealing.

According to Fig. 2, La-rich regions are correlated with  $\alpha$ -Al nanocrystals. As demonstrated in Fig. 3, this is due to the presence of a La-rich shell around the  $\alpha$ -Al nanocrystals, containing more than 12 at. % of La. Figures 3(a) and 3(b) show a two-dimensional (2D) section of the atom positions of Al in  $\alpha$ -Al and La in La rich regions inside a volume of the glass annealed at 443 K for 2 h. It is clearly visible that  $\alpha$ -Al nanocrystals are surrounded by a La shell of a few nanometers width. Analysis of further 2D sections through the analyzed volume confirms this picture. This result is in accordance with a previous study based on small-angle neutron scattering suggesting that such a core-shell structure could exist in the annealed  $\text{Al}_{89}\text{Ni}_6\text{La}_5$  glass.<sup>7</sup> The neutron scattering data obtained from this glass aged up to 453 K

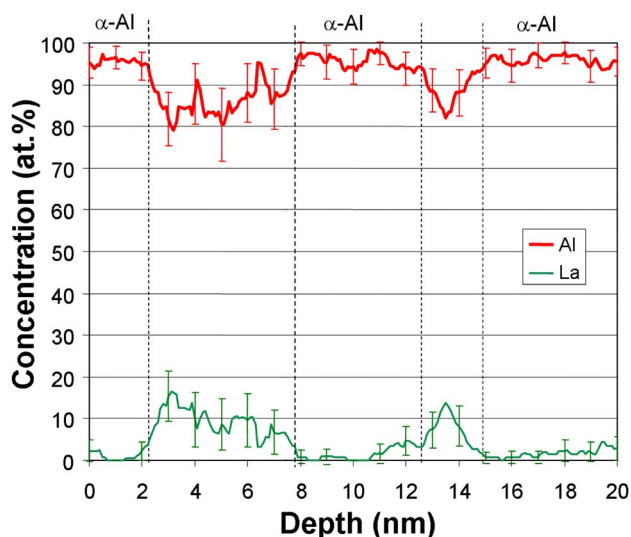


FIG. 4. (Color online) Concentration depth profiles of Al and La along the axis of the cylinder of 1 nm diameter shown in Fig. 3(a). The vertical dashed lines indicate interfaces between  $\alpha$ -Al crystal and amorphous phase.

could be fitted by two distributions of spherical fluctuations which were interpreted either as core-shell structures with pure Al particles forming the core, or by two different particles that grow independently. The present investigation demonstrates that core-shell structures actually exist.

Figure 4 shows AP concentration depth profiles of Al and La taken along the axis of the cylinder of 1 nm diameter marked in Fig. 3(a). This cylinder cuts out a region of the annealed material that contains some Al nanocrystals and La-rich regions at their interfaces. The width of the  $\alpha$ -Al nanocrystal between two La-rich areas is approximately 5 nm, while the La-rich areas are 2.5 and 5 nm thick. In the latter case, the La shells around two  $\alpha$ -Al nanocrystals have merged to one layer with a La concentration above 15 at. %.

The present investigations demonstrate that nanocrystallization of Al and growth of these crystallites require the rejection of La. The enrichment of La at the interface of crystalline clusters indicates the low mobility of La in the amorphous parent phase. This in turn hinders the growth of the  $\alpha$ -Al nanocrystals. The diffusion of alloying elements in metallic glasses is known to be sensitive to the relative size of the diffusing and the host atoms.<sup>18</sup> The low mobility of La can be explained by its larger atomic radius (0.1879 nm) compared to Ni (0.124 nm) and Al (0.143 nm). Thus, the growth velocity and the final size of the  $\alpha$ -Al crystals are controlled by the diffusion of La into the amorphous matrix. Regions where La shells around various  $\alpha$ -Al nanocrystals

have merged should be even higher barriers for the growth of these  $\alpha$ -Al crystals.

In summary, the present 3D-AP investigation of the early stages of crystallization of  $\text{Al}_{89}\text{Ni}_6\text{La}_5$  metallic glass demonstrates that both minor components Ni and La have a crucial influence on the evolution of  $\alpha$ -Al nanocrystals in Al–Ni–La metallic glasses. Even the as-quenched material shows inhomogeneities of the Ni and Al atom distribution on the nanoscale. The Al-rich regions act as nucleation sites of  $\alpha$ -Al nanocrystals during annealing in the temperature range of the first crystallization step. During crystallization, La-rich shells around  $\alpha$ -Al particles build up when La atoms are rejected from the growing crystals of almost pure  $\alpha$ -Al. These shells hinder further growth and, thus, limit the size of the  $\alpha$ -Al nanocrystals. Our investigation confirms the existence of core-shell structures and proved this previously postulated pathway of nanocrystallization.

The authors gratefully thank Dr. M.-P. Macht and Dr. Ch. Abromeit for fruitful discussions.

- <sup>1</sup>A. Inoue, K. Ohtera, A. P. Tsai, and T. Masumoto, *Jpn. J. Appl. Phys., Part 2* **27**, L479 (1988).
- <sup>2</sup>G. Wilde, N. Boucharat, R. J. Hebert, H. Rösner, W. S. Tong, and J. H. Perepezko, *Adv. Eng. Mater.* **5**, 125 (2003).
- <sup>3</sup>Y. H. Kim, A. Inoue, and T. Masumoto, *Mater. Trans., JIM* **32**, 599 (1991).
- <sup>4</sup>H. Nitsche, F. Sommer, and E. J. Mittemeijer, *J. Non-Cryst. Solids* **351**, 3760 (2005).
- <sup>5</sup>Z. H. Huang, J. F. Li, Q. L. Rao, and Y. H. Zhou, *Intermetallics* **15**, 1139 (2007).
- <sup>6</sup>V. Ronto, L. Battezzati, A. R. Yavari, M. Tonegaru, N. Lupu, and G. Heunen, *Scr. Mater.* **50**, 839 (2004).
- <sup>7</sup>K. L. Sahoo, M. Wollgarten, J. Haug, and J. Banhart, *Acta Mater.* **53**, 3861 (2005).
- <sup>8</sup>J. H. Perepezko, R. J. Hebert, and G. Wilde, *Mater. Sci. Eng.* **375-377**, 171 (2004).
- <sup>9</sup>K. F. Kelton, T. K. Croat, A. K. Gangopadhyay, L.-Q. Xing, A. L. Greer, M. Weyland, X. Li, and K. Rajan, *J. Non-Cryst. Solids* **317**, 71 (2003).
- <sup>10</sup>D. Isheim, D. N. Seidman, J. H. Perepezko, and G. B. Olson, *Mater. Sci. Eng., A* **353**, 99 (2003).
- <sup>11</sup>T. Gloriant, D. H. Ping, K. Hono, A. L. Greer, and M. D. Baró, *Mater. Sci. Eng., A* **304-306**, 315 (2001).
- <sup>12</sup>P. Rizzi, M. Baricco, L. Battezzati, P. Schumacher, and A. L. Greer, *Mater. Sci. Forum* **235-238**, 409 (1997).
- <sup>13</sup>A. P. Tsai, Y. Kamiyama, A. Inoue, and T. Masumoto, *Acta Mater.* **45**, 1477 (1997).
- <sup>14</sup>N. Wanderka, B. Radiguet, K. L. Sahoo, D. Blavette, and J. Banhart (to be published).
- <sup>15</sup>D. Blavette, B. Deconihout, A. Bostel, J. M. Sarrau, M. Bouet, and A. Menand, *Rev. Sci. Instrum.* **64**, 2911 (1993).
- <sup>16</sup>W. Lefebvre, G. Dacosta, F. De Geuser, A. Deschamps, and F. Danoix, *Surf. Interface Anal.* **39**, 206 (2007).
- <sup>17</sup>N. Wanderka, B. Radiguet, K. L. Sahoo, and J. Banhart, *Mater. Sci. Forum* **539-543**, 1917 (2007).
- <sup>18</sup>F. Faupel, W. Frank, M.-P. Macht, H. Mehrer, V. Naundorf, K. Rätzke, H. Schober, S. Sharma, and H. Teichler, *Rev. Mod. Phys.* **75**, 237 (2003).